



A Kinetics of Hydrogen Reduction of Nickel Oxide at Moderate Temperature

Dong Soo Lee¹ · Dong Joon Min¹

Received: 4 December 2018 / Accepted: 7 March 2019 / Published online: 19 March 2019
© The Author(s) 2019

Abstract

Nano-metallic nickel powders are highly-valued materials applied in energy, electronic devices and aerospace, which is known to be produced by the gaseous phase reduction method of NiCl_2 . In the case of a gaseous reduction method, size control is difficult due to the agglomeration of nickel powders. Therefore, a method of producing highly-valued nickel nano-powders from $\text{Ni}(\text{OH})_2$ has been proposed. Considering the reduction behavior of bulk nickel oxide has been reported to follow the topo-chemical model. However, reduction behavior of nano-particle is expected to be unknown state. It is necessary to clarify the mechanism of nickel oxide nano-particle reduction. Therefore, in this study, the temperature dependence and particle size dependence on the reduction behavior of from micro scale to nano scale particle was confirmed through TGA experiment. Also, the reduction mechanism of nickel oxide powder was also investigated based on kinetic considerations using the grain topo-chemical model. It was confirmed that the reduction reaction of nickel oxide powder undergoes through the 2nd Avrami model and reduction rate can be expressed by function of temperature and particle size of the powder. Due to the part of the diffusion, the particle size of the powder also affects the rate constant of the reduction reaction.

$$g_{(x)} = k \cdot f(d) \cdot t$$

Keywords Kinetics · Reduction mechanism · Hydrogen reduction · Nickel oxide · Reduction equation

1 Introduction

Nickel powder is mainly used for nickel–cadmium batteries, nickel hydrogen batteries, and multi-layer ceramic capacitors [1, 2]. Conventional process for making nickel powder can be represented by hydrothermal process and chemical deposition process. But hydrothermal process has uneven growth of particles and chemical vapor deposition has the agglomeration problem, which causes production decreases.

A novel flash ironmaking process developed at the University of Utah [3–8], expected to solve these problems. In flash ironmaking process, drop tube furnace is used to reduce nickel oxide to be reduced by hydrogen gas. But in the case of drop tube furnace, reduction time limited as traveling time. So reduction mechanism should be analyzed, and can be predicted.

By the thermochemical approach, the reduction of nickel oxide by hydrogen is identified particularly suitable in some kinetics and mechanical models [9–20].

Benton and Emmett [9] established some characteristics such as boundary layer reduction, autocatalytic reaction, incubation period, effect of water vapor.

After that Richardson et al. [16, 17] found that nickel oxide reduction follows homogeneous reaction process, in the temperature range from 448 to 1173 K. And showed the 1st order reaction model is suitable.

Utigard et al. [18] studied the reduction reaction of nickel oxide in the temperature range from 823 to 1273 K. And found that interfacial chemical reaction act as a rate determining step.

Plascencia and Utigard [19] reduced nickel oxide by hydrogen in the temperature range from 623 to 1273 K. Interfacial chemical reaction and the mass transport of reducing gas and product gas can be defined as a rate determining step. And also find out that the size of nickel oxide powder can make difference in reduction rate constant.

But the influence of particle size is not taken into account in the reduction equation. So, there is a limit to predict the reaction behavior.

✉ Dong Joon Min
chemical@yonsei.ac.kr

¹ Department of Material Science and Engineering, Yonsei University, 50 Yonsei-Ro, Seodaemun-Gu, Seoul 038722, Republic of Korea

Therefore, in this study, it is aimed to investigate the influence of temperature and particle size on the reduction process. In order to consider the influence of particle size in the calculation of the reduction rate, consideration is given to the function of the particle size as in Eq. (1)

$$g_{(x)} = k \cdot f(d) \cdot t \tag{1}$$

2 Experimental

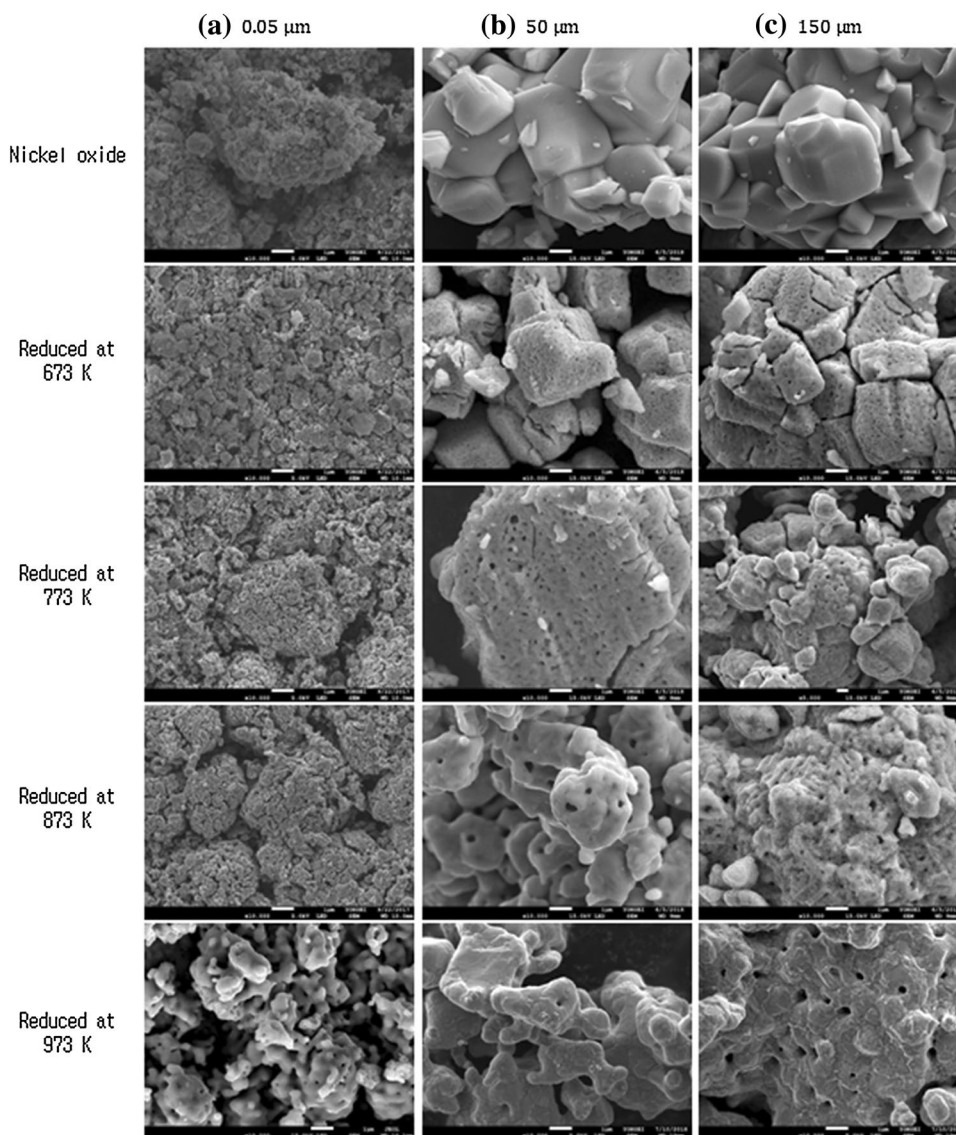
2.1 Sample Preparation

In order to minimize the influence of impurities, a reagent grade nickel oxide powder of 0.05 μm was used. To

examine the effect of powder particle size dependence, nickel powder having a particle size of 50 μm, 150 μm was used after oxidation. The powder samples of nickel oxide are shown in Fig. 1, which shows dense phase.

For the reduction experiment, Thermo-gravimetric analysis (TGA, Setaram) was used. And 0.5 g of nickel oxide powder was pressed into a pellet shape with a force of 1 ton in a cylindrical mold, and a small amount of alcohol was used for adhesion. The pressed nickel oxide pellet was dried in a drying oven at a temperature of 423 K for 24 h in order to remove the residual moisture and used alcohol in the pellet. All of the nickel oxide pellet produced in the same size (diameter 10 mm, height 3 mm).

Fig. 1 SEM image of nickel oxide sample for each particle size **a** 0.05 μm, **b** 50 μm, **c** 150 μm



The reduction reaction was carried out using 100% hydrogen gas, in the temperature range from 673 to 973 K.

2.2 Apparatus and Procedure

By using Thermo-gravimetric analysis (TGA, SETSYS Evolution, Setaram) shown in Fig. 2. The weight change during the reduction reaction was recorded at 1 Hz intervals. The nickel oxide pellet proceeded through the same experimental steps as follows.

Step I Temperature raising in a high purity Ar(6 N) atmosphere.

Step II After reaching the target temperature, it maintains a certain time to stabilize the PID.

Step III Reduction reaction starts by gas changes from Ar to H₂.

After the nickel oxide pellets reached their respective target temperatures (673 K–973 K), the reduction reaction proceeded by hydrogen gas at isothermal temperature. The sample after the reduction was quenched in an Ar atmosphere. Based on the experimental data, the reduction degree can be defined as

$$R(\%) = \frac{\Delta W_{\text{O}}^t}{W_{\text{O}}^i} \times 100, \quad (2)$$

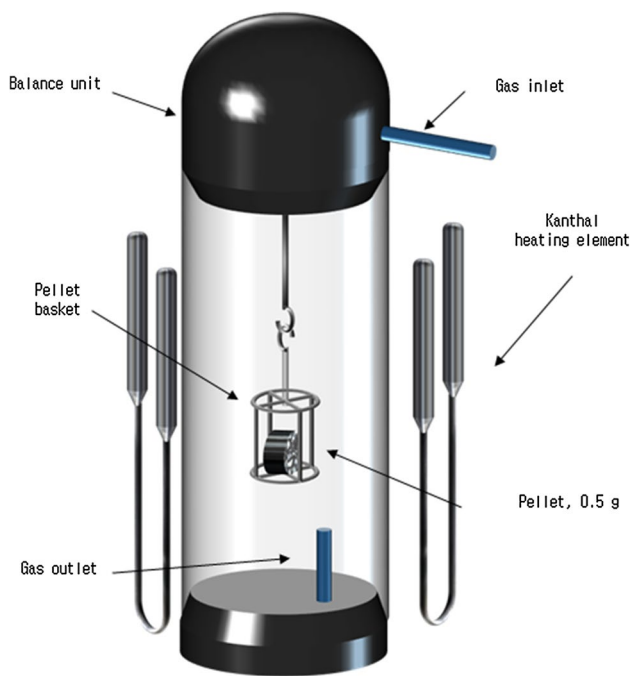


Fig. 2 Schematic diagram of the TGA

where W_{O}^i is the amount of removable oxygen in the initial sample and ΔW_{O}^t is the weight of oxygen removed at time t . Obtained sample was observed by scanning electron microscopy (SEM, SM-7001F, JEOL).

In step III, which is reduction reaction starts by gas changes from Ar to H₂, corresponds to the initial section of general reduction curve. The initial section called incubation period. In this process the atmosphere changes from the inert gas(Ar) to reducing gas(H₂). This incubation period excluded from the mathematical modeling process because it is affected by hydrogen partial pressure. And also, in the case of the diffusion rate period, the gas diffusion at the end of reduction and inside of the product means a section that acts as a rate controlling step [21]. This study aims at the kinetic analysis of the reduction reaction period and to investigate the influence of temperature and particle size during the reduction period. Therefore, we investigated the mathematical interpretation of the reduction period, where the reduction reaction takes place.

3 Results and Discussion

3.1 Reduction Behavior of Nickel Oxide Under H₂ Gas by Using TGA Method

Figure 3 shows the reduction degree(R) and the reaction time(t) calculated through Eq. (2) for the reduction temperature of each particle size of nickel oxide. And it is confirmed that the reduction rate becomes faster as the reduction temperature increases. It can be seen that reduction rate increases remarkably with decreasing particle size from micro scale to nano scale compared to the effect of the reduction temperature.

It can be seen that there is an incubation period caused by changing of the gas atmosphere at all temperature ranges. In addition, the inflection point of the reduction curve can be observed at the end of the reaction. After the inflection point, the diffusion acts as the rate determining step. So, only the reduction period excluding the incubation period and the diffusion rate period was analyzed.

The behavior of the reduction mechanism during the reduction period can be interpreted based on grain model mentioned in Szekely et al. [22]. Based on the grain model, reduction conversion equations, which are described in Table 1, are applied to the reduction of nickel oxide and plotted in Fig. 4. In order to find out a suitable model, R² value is calculated by linear approximation and results are shown in Table 1. Recently, the reduction reaction of oxides has been analyzed by the nucleation and growth. In this paper, Avrami model is confirmed to be the suitable model [23–26]. Figure 1 shows an SEM image of the surface shape of nickel after reduction. Through this, it

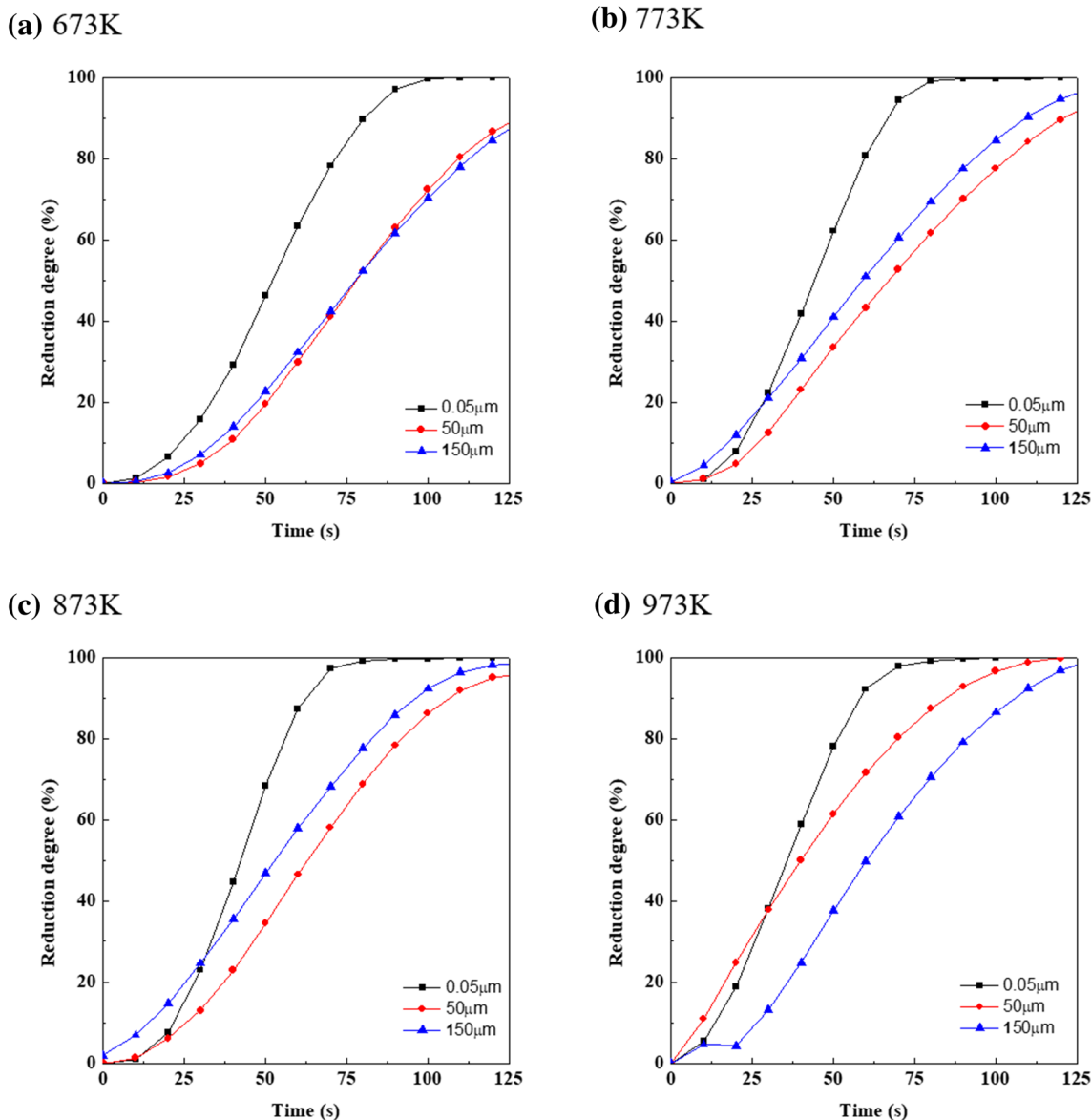


Fig. 3 Reduction degree of nickel oxide (NiO) powder pellet by hydrogen at each reduction temperature **a** 673 K, **b** 773 K, **c** 873 K, **d** 973 K

can be confirmed that the reaction proceeds by nucleation and growth [27]. Therefore, the reduction behavior of nickel oxide with respect to hydrogen can be expressed as Eq. (3).

$$g(x) = [-\ln(1 - x)]^{\frac{1}{n}} = k \cdot f(d) \cdot t = k_{app} \cdot t \quad (3)$$

The purpose of this study is to suggest an overall reduction equation for powder reduction and therefore to

use the Avrami 2nd model, which has the most common concordance.

3.2 Temperature Dependence on the Reduction Equation

Applying the Avrami 2nd model, the graph of $g(x) = [-\ln(1 - x)]^{\frac{1}{2}}$ and t according to each particle size

Table 1 Differential and integral form of various models

Model	Differential form $f(x) = \frac{1}{k} \frac{dx}{dt}$	Integral form $g(x) = kt$	R ²
Diffusion model			
10 diffusion (10)	1/(2x)	x ²	0.911
20 diffusion (20)	-[1/ln(1-x)]	((1-x)ln(1-x)) + x	0.861
30 diffusion (30)	$\left[3(1-x)^{\frac{2}{3}}\right] / \left[2\left(1-(1-x)^{\frac{1}{3}}\right)\right]$	$\left(1-(1-x)^{\frac{1}{3}}\right)^2$	0.755
Nucleation model			
Avrami–Erofeev (A2)	$2(1-x)[-ln(1-x)]^{\frac{1}{2}}$	$[-ln(1-x)]^{\frac{1}{2}}$	0.984
Avrami–Erofeev (A3)	$3(1-x)[-ln(1-x)]^{\frac{2}{3}}$	$[-ln(1-x)]^{\frac{1}{3}}$	0.977
Avrami–Erofeev (A2)	$4(1-x)[-ln(1-x)]^{\frac{3}{4}}$	$[-ln(1-x)]^{\frac{1}{4}}$	0.951
Interfacial chemical reaction model			
Contracting area (R2)	$2(1-x)^{1/2}$	$1-(1-x)^{1/2}$	0.944
Contracting volume (R3)	$3(1-x)^{2/3}$	$1-(1-x)^{1/3}$	0.944

and temperature in shown as Fig. 4 respectively. The slope of the graph can be represented by $\frac{g(x)}{t}$, which is expressed as the apparent rate constant k_{app} .

$$k = \frac{k_{app}}{f(d)} \quad (4)$$

$$k = A \cdot \exp\left(-\frac{E_a}{RT}\right) \quad (5)$$

$$\ln k = \ln A - \frac{E_a}{RT} \quad (6)$$

For k_{app} , it can be expressed as $\exp\left(-\frac{E_a}{RT}\right)$ in the Arrhenius equation. Since the particle size is fixed at this time, the function $f(d)$ for the particle size is included in the collision factor constant A. Combining from Eqs. (4)–(5), the Arrhenius graph for the hydrogen reduction of nickel oxide is shown as Fig. 5 in temperature range of 673–973 K. It has three activation energy values according to three particle sizes (0.05 μm , 50 μm , 150 μm), and it can be confirmed that it has three A value in the same manner. Therefore, the hydrogen reduction reaction formula of nickel oxide in the following Eq. (7)

$$g(x) = [-\ln(1-x)]^{\frac{1}{2}} = k \cdot f(d) \cdot t = A \cdot \exp\left(-\frac{E_a}{RT}\right) \cdot f(d) \cdot t \quad (7)$$

$$\begin{aligned} A &= 0.0614, E_a = 6.448 \text{ kJ (for } 0.05 \mu\text{m)} \\ A &= 0.0455, E_a = 8.406 \text{ kJ (for } 50 \mu\text{m)} \\ A &= 0.0200, E_a = 3.367 \text{ kJ (for } 150 \mu\text{m)}. \end{aligned}$$

3.3 Particle Size Dependence on the Reduction Equation

The effect of the particle size on the reduction at different reduction temperatures is also shown if Fig. 4 when the reduction temperature in determined, it has a different slope value depending on the particle size of each powder, and the slope can be expressed as $k \cdot f(d)$. As the reduction temperature increases from 673 K to 973 K, it can be confirmed that the influence on particle size is different.

The value for n can be obtained through the slope of Fig. 4, assuming that the particle size effect on the reduction rate is $f(d) = d^n$.

$$\text{slope of Fig. 4} = k_{app} = k \cdot f(d) = k \cdot d^n \quad (8)$$

$$\ln(k_{app}) = \ln k + n \ln d \quad (9)$$

A graph showing the x-axis as $\ln d$ and y-axis as $\ln(k \cdot f(d))$ for Eq. (9) at different reaction temperatures is shown as Fig. 6, and the slope indicates the value of n . The value of n also tends to increase as the reduction temperature increases, indicating that the influence on the particle size increases with increasing temperature. Therefore, in order to express n as an equation for temperature, a graph having a temperature and n as an axis can be expressed as Fig. 7 With this graph, n can be expressed as Eq. (10) by linear approximation

$$n = 17.68 \frac{1}{T} - 0.1057 \quad (10)$$

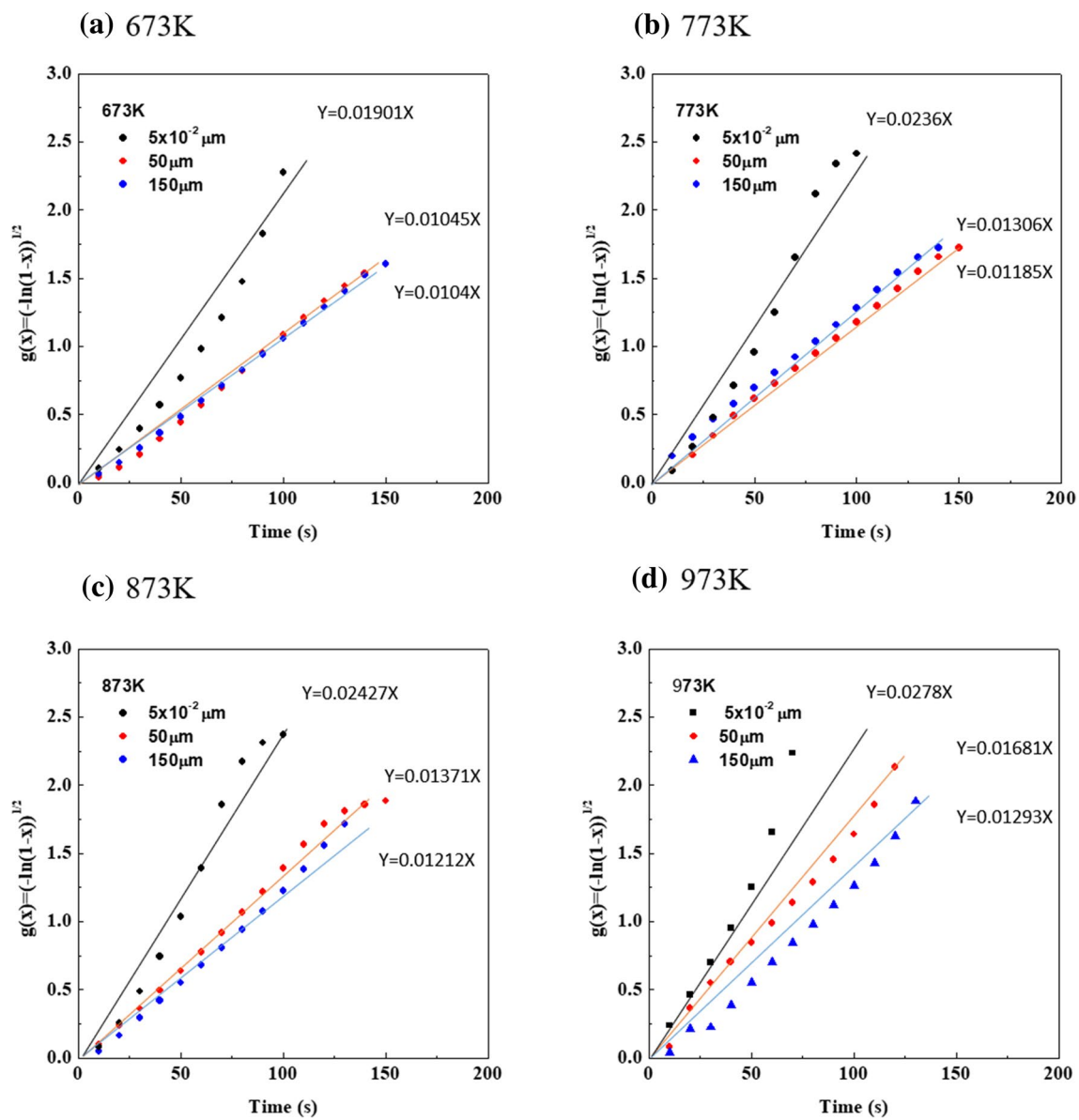


Fig. 4 Relationship between $[-\ln(1-x)]^{1/2}$ and reduction time **a** 673 K, **b** 773 K, **c** 873 K, **d** 973 K

So, the equation for hydrogen reduction of nickel oxide can be formulated as following Eq. (11)

$$[-\ln(1-x)]^{1/2} = A \cdot \exp\left(-\frac{E_a}{RT}\right) \cdot d^{17.68\frac{1}{T}-0.1057} \cdot t \quad (11)$$

3.4 Comparison of Calculated and Experimental Data

The reduction equation obtained through this study was

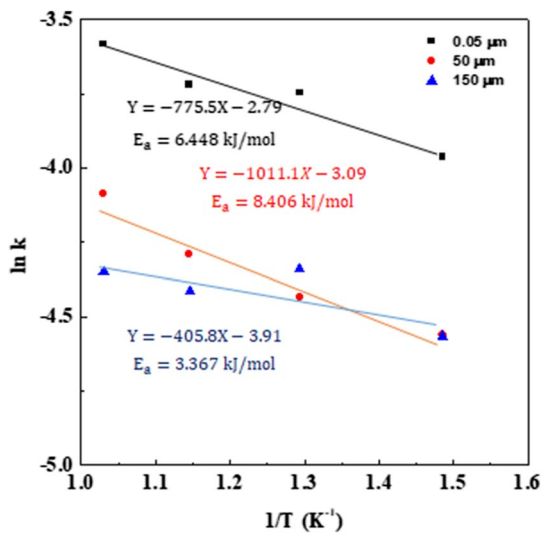


Fig. 5 Arrhenius plot between $\ln k$ and $1/T$

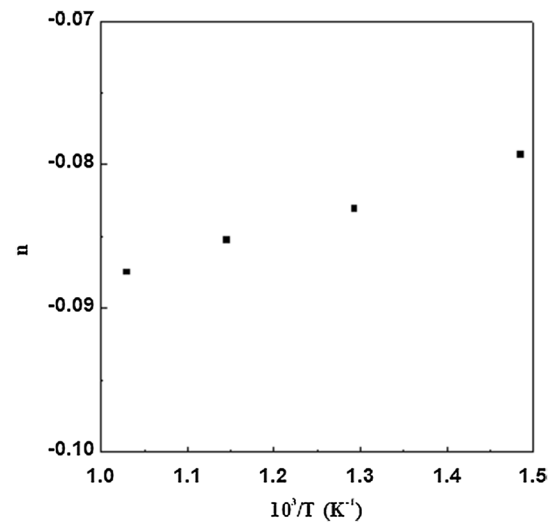


Fig. 7 The relationship between n and temperature

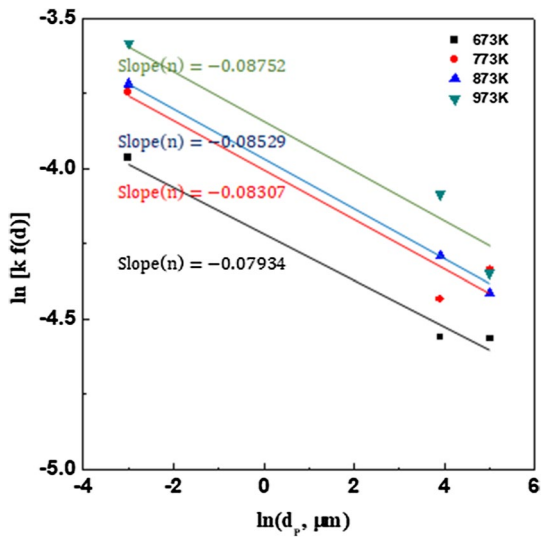


Fig. 6 The relationship between d and $k \cdot f(d)$ from 673 to 973 K

compared with the values obtained through experiments. The reliability was verified by comparing the reduction rates. The experimental data were derived from the slope of the time vs reduction degree plot (Fig. 3). The Eq. (12) obtained by differentiating the suggested reduction equation Eq. (11).

$$\frac{dx}{dt} = 2 \cdot A \cdot \exp\left(-\frac{E_a}{RT}\right) \cdot d^{17.68 \frac{1}{T} - 0.1057} \cdot (1 - X) \cdot [-\ln(1 - X)]^{\frac{1}{2}} \quad (12)$$

At 773 K, reduction rates vs time can be plotted as Fig. 8. And it can be seen that the tendency of the reduction rate obtained by the experiment and calculation are in agreement with each other.

The purpose of this study was to predict the reduction rate with varying particle size and to predict the time, temperature and reduction degree. In the drop tube furnace, the reduction time is determined according to the falling velocity of the powder, and it is expected that the reduction conditions to obtain the target reduction rate can be predicted (Fig. 9).

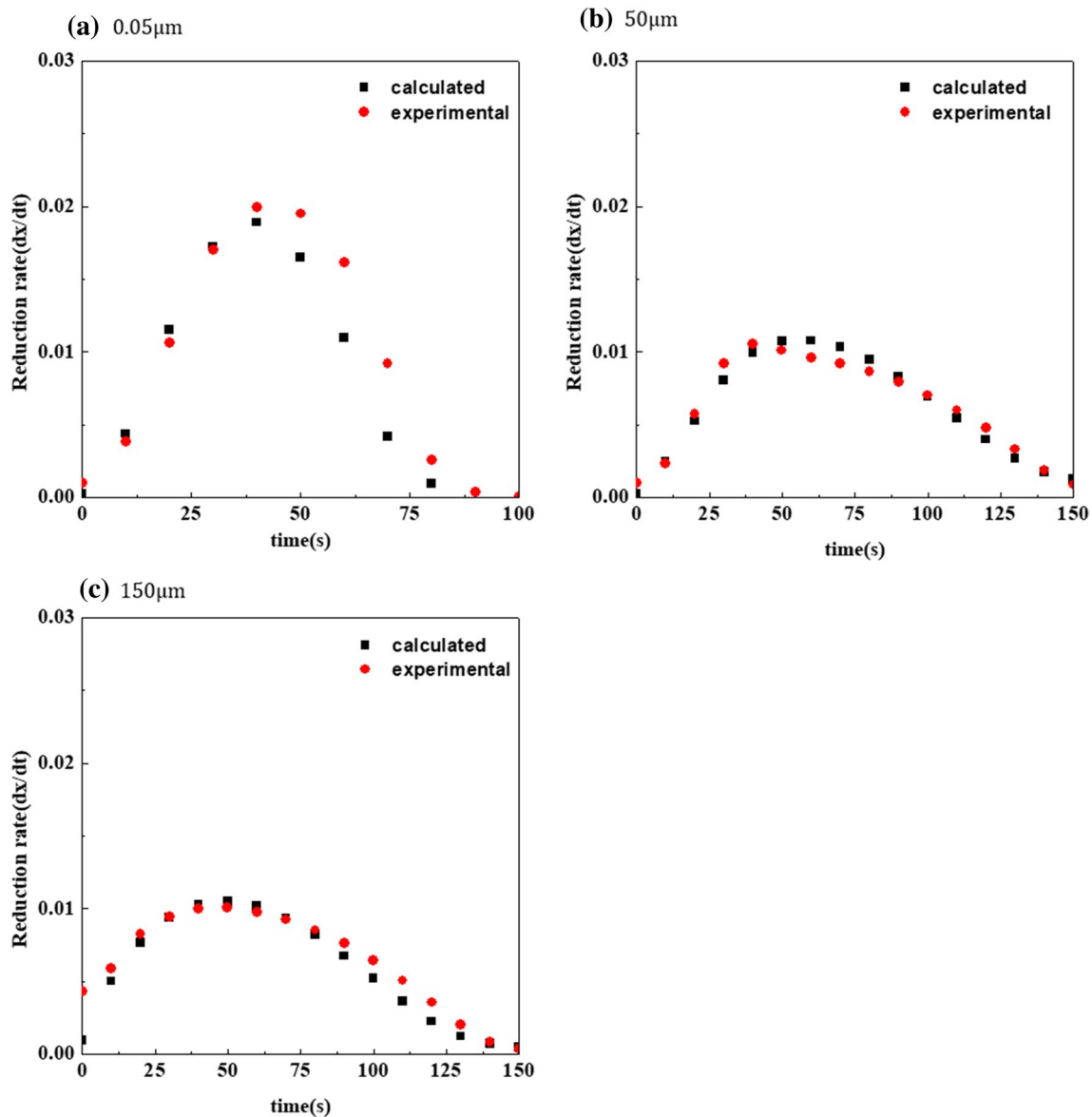


Fig. 8 Comparison of calculated and experimental reduction rate versus time plot **a** 0.05 μm , **b** 50 μm , **c** 150 μm at 773 K

4 Conclusion

The aim of this experiment was to predict the reduction rate of nickel oxide powders by changing the particle size and temperature.

The hydrogen reduction of nickel oxide was proceeded through TGA, and reduction modeling was applied through the obtained reduction degree graph. The Avrami 2nd model

was found to be most suitable for defining the reduction equation for the whole region. Through the mathematical modeling, the reduction equation for the hydrogen reduction of nickel oxide can be derived. So that a condition for obtaining a desired reduction degree within a predetermined time can be obtained.

Because the incubation period is ignored in calculated results. So there is tendency the experiment results show higher degree at the start of reduction. At the end of the

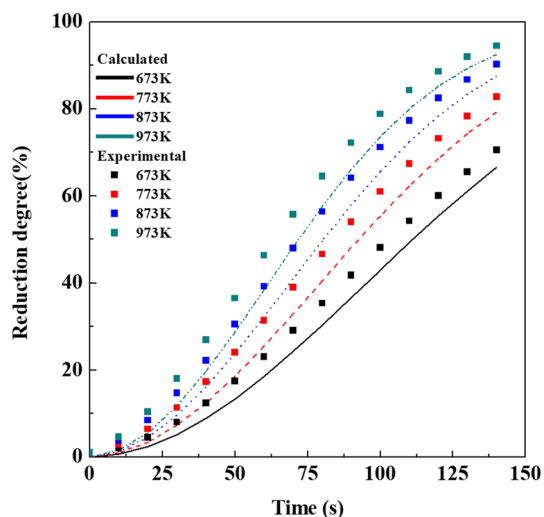


Fig. 9 Comparison of calculated and experimental reduction degree versus time plot for 50 μm at each temperature

reduction, which is caused by diffusion rate period, the experimental reduction rate shows slow down.

Acknowledgements This work was supported by the Ministry of Trade, Industry and Energy under Project No. 10077986. This work was supported by the third stage of Brain Korea 21 Plus Project in Division of Creative Materials.

Open Access This article is distributed under the terms of the Creative Commons Attribution 4.0 International License (<http://creativecommons.org/licenses/by/4.0/>), which permits unrestricted use, distribution, and reproduction in any medium, provided you give appropriate credit to the original author(s) and the source, provide a link to the Creative Commons license, and indicate if changes were made.

References

1. Battery Association of Japan. 10 (2011)

2. Jfe Technical report. **6**, 71, (2005)
3. M.E. Choi, H.Y. Sohn, *Ironmak. Steelmak.* **37**, 81 (2010)
4. H.K. Pinegar, M.S. Moats, H.Y. Sohn, *Steel Res. Int.* **82**, 951 (2011)
5. H.Y. Sohn, *Steel Times Int.* **31**, 68 (2007)
6. M.Y. Mohassab-Ahmed, H.Y. Sohn, *JOM* **65**, 1559 (2013)
7. M.Y. Mohassab-Ahmed, H.Y. Sohn, *Steel Res. Int.* **85**, 875 (2014)
8. M.Y. Mohassab-Ahmed, H.Y. Sohn, *Ironmak. Steelmak.* **41**, 665 (2014)
9. A.F. Benton, P.H. Emmett, *J. Am. Chem. Soc.* **46**, 2728 (1924)
10. A. Kivnick, A.N. Hixson, *Chem. Eng. Prog.* **48**, 394 (1952)
11. G. Parravano, *J. Am. Chem. Soc.* **74**, 1194 (1952)
12. A. Yamaguchi, J. Moriyama, *Jpn. Inst. Met.* **28**, 692 (1964)
13. T. Kurosawa, R. Hasegawa, T. Yagihashi, *Trans. Jpn. Inst. Met.* **13**, 265 (1972)
14. C.I. Szekely, H.Y. Lin, A. Soh, *Chem. Eng. Sci.* **28**, 1975 (1973)
15. J.W. Evans, K. Haase, *High Temp Sci.* **8**, 167 (1976)
16. J.T. Richardson, R. Scates, M.V. Twigg, *Appl. Catal. A* **246**, 137 (2003)
17. J.T. Richardson, R. Scates, M.V. Twigg, *Appl. Catal. A* **267**, 35 (2004)
18. T.A. Utigard, M. Wu, G. Plascencia, T. Martin, *Chem. Eng. Sci.* **60**, 2061 (2005)
19. G. Plascencia, T.A. Utigard, *Chem. Eng. Sci.* **64**, 3879 (2009)
20. B.V. L'vov, A.K. Galwey, *J. Therm. Anal. Calorim.* **110**, 601 (2012)
21. W.H. Kim, S.M. Lee, S.M. Kim, D.J. Min, *Int. J. Hydrogen Energy* **38**, 4194 (2013)
22. J. Szekely, C.I. Lin, H.Y. Sohn, *Chem. Eng. Sci.* **18**, 48 (1973)
23. M. Avrami, *J. Chem. Phys.* **7**, 1103 (2004)
24. M. Avrami, *J. Chem. Phys.* **8**, 212 (2004)
25. M. Avrami, *J. Chem. Phys.* **9**, 177 (2004)
26. A. Khawam, D.R. Flanagan, *J. Phys. Chem. B.* **110**, 17315 (2006)
27. M.E. Brown, *Introduction to Thermal Analysis: Techniques and Applications* (Kluwer, Dordrecht, 2001)

Publisher's Note Springer Nature remains neutral with regard to jurisdictional claims in published maps and institutional affiliations.